# Extensive release of methane from Arctic seabed west of Svalbard during summer 2014 does not influence the atmosphere

C. Lund Myhre[1], B. Ferré[2], S. M.Platt[1], A. Silyakova[2], O. Hermansen[1], G. Allen[3], I. Pisso[1], N. Schmidbauer[1], A. Stohl[1], J. Pitt[3], P. Jansson[2], J. Greinert[8,2], C. Percival[3], A. M. Fjaeraa[1], S. O'Shea[3], M. Gallagher[3], M. Le Breton[3], K. Bower[3], S. Bauguitte[7], S. Dalsøren[4], S. Vadakkepuliyambatta[2], R. E. Fisher[6], E.G. Nisbet[6], D. Lowry[6], G.Myhre[4], J. Pyle[5], M. Cain[5], J. Mienert[2]

1 NILU - Norwegian Institute for Air Research, PO Box 100, 2027 Kjeller, Norway

2 CAGE-Centre for Arctic Gas Hydrate, Environment and Climate, Department of Geology, University of Tromsø, 9037 Tromsø, Norway

3 School of Earth, Atmospheric and Environmental Science, University of Manchester, Oxford Rd, Manchester, M13 9PL, UK.

4 Center for International Climate and Environmental Research – Oslo (CICERO), Pb. 1129 Blindern, 0318 Oslo, Norway

5 National Centre for Atmospheric Science, Department of Chemistry, University of Cambridge, Lensfield Road, Cambridge CB2 1EW, UK

6 Royal Holloway, University of London, Egham, Surrey, TW20 0EX, UK

7 Facility for Airborne Atmospheric Measurements (FAAM), Building 125, Cranfield University, Cranfield, Bedford, MK43 0AL, UK

8 GEOMAR, Helmholtz-Zentrum für Ozeanforschung, Wischhofstr. 1-3, 24148 Kiel, Germany

Corresponding author: Cathrine Lund Myhre (clm@nilu.no)

**Key Points:**

- Summer 2014 $CH_4$ release from seabed sediments west of Svalbard substantially increases $CH_4$ concentrations in the ocean, but not in the atmosphere
- The maximum flux to the atmosphere compatible with the observed atmospheric $CH_4$ mixing ratios is 2.4-3.8 nmol m$^{-2}$ s$^{-1}$ from 20 June – 1 August 2014
- Ay ocean-atmosphere flux of the $CH_4$ accumulated beneath the pycnocline may only occur if physical processes remove this dynamic barrier

44

**Abstract**

46 We find that summer methane ($CH_4$) release from seabed sediments west of Svalbard
47 substantially increases $CH_4$ concentrations in the ocean, but has limited influence on the
48 atmospheric $CH_4$ levels. Our conclusion stems from complementary measurements at the sea
49 floor, in the ocean, in the atmosphere from land-based, ship and aircraft platforms during a
50 summer campaign 2014. We detected high concentrations of dissolved $CH_4$ in the ocean above
51 the seafloor with a sharp decrease above the pycnocline. Model approaches taking potential $CH_4$
52 emissions from both dissolved and bubble released $CH_4$ from a larger region into account, reveal
53 a maximum flux compatible with the observed atmospheric $CH_4$ mixing ratios of 2.4-3.8 nmol
54 $m^{-2}$ $s^{-1}$. This is too low to have an impact on the atmospheric summer $CH_4$ budget in the year
55 2014. Long-term ocean observatories may shed light on the complex variations of Arctic $CH_4$
56 cycles throughout the year.

57

# 1  Introduction

The important greenhouse gas methane ($CH_4$) has large natural sources vulnerable to climate change [Ciais et al., 2013, Myhre et al., 2013, Portnov et al., 2016]. The causes of the recent global average growth of ~6 ppb year$^{-1}$ since 2007 in atmospheric $CH_4$, including a marked Arctic growth event in 2007, remain unclear [Nisbet et al, 2014, Kirschke et al. 2013]. Decomposing methane hydrates (MHs) in marine sediments along continental margins are potentially a large natural source [Ruppel et al 2011]. How much of the $CH_4$ stored or formed by biogenic processesin the Arctic subsea that escapes to the atmosphere remains an open question. Large $CH_4$ gas escape from the shallow seabed into the ocean column has been reported from East Siberian shelves, particularly during storms [Shakhova et al., 2014], and from the Laptev and Kara Seas [Shakhova et al. 2010, Portnov et al., 2013]. Very high fluxes of $CH_4$ from sub-seabed sources to the atmosphere have been reported for the East Siberian Arctic Shelf (ESAS) [Shakhova et al. 2014, 2010], with flux values of ca. 70-450 nmol m$^{-2}$ s$^{-1}$ under windy conditions, with a postulated average total area (extrapolated) source magnitude of 17 Tg year$^{-1}$ representing 3% of the global budget to the atmosphere. However, on the contrary it was recently found that ESAS region only emits from 0.5 to 4.5 Tg year$^{-1}$ (Berchet et al. 2016). Based on continuous atmospheric observations.There are hundreds of gas plumes observed in the water, suggestive of gas release north-west off Svalbard. Along the West Svalbard continental margin, extensive gas bubbling from the sea floor has been observed in shallow water at 90-400 m depth [this work, Knies et al., 2004; Westbrook et al, 2009; Rajan et al., 2012, Sahling et al., 2014; Veloso et al., 2015; Graves et al., 2015; Steinle et al., 2015, Portnov et al., 2016] outside of today's gas hydrate stability zone [Panieri et al., 2016]. It is unknown how much of the $CH_4$ flux from the marine sediments in this region ultimately reaches the atmosphere [Fisher et al., 2011], either through bubbles or flux of dissolved $CH_4$.

The amount of $CH_4$ stored within gas hydrates, or as dissolved and free gas, north of 60$^{o}$N is uncertain. Estimates as high as 1200 Gt have been reported [Biastoch et al 2011]. Some hydrate deposits may be on the verge of instability due to ocean warming, leading to a debate whether $CH_4$ release could trigger positive feedback and accelerate climate warming [Archer, 2007, Isaksen et al, 2011; Ferré et al., 2012]. There have been very few studies aimed at detecting and quantifying the potential atmospheric enhancement of this oceanic source around Svalbard, and estimating their fluxes contributions. The West Svalbard continental margin is warmed by the northward flowing West Spitsbergen Current, the northernmost limb of the Gulf Stream. There has been an increase in the bottom water temperature in this area of 1.5 ℃ [Ferré et al, 2012] over the last 30 years, while the atmosphere has warmed by as much as 4 ℃ since the early 1970s [Nordli et al, 2014]. Continued warming in this region is expected [Collins et al, 2013]. Consequently, it is crucial to determine whether, and how, $CH_4$ from the shallow shelf located close to a stable gas hydrate zone on the upper continental margin reaches the atmosphere at present, and how this might change in the future. To investigate this we have conducted an intensive atmospheric and oceanographic survey (Figure 1) in an area with a known high density of hydroacostically detected gas flares (indications of bubbles in echograms) west of Prins Karls Forland, Svalbard, from 23 June to 2 July 2014, with atmospheric measurements continuing to 1 August. We investigated whether there was an atmospheric enhancement and impact during summer time. The measurements were used in combination with three different models to provide independent top down flux constraints, also taking into account potential emissions from larger areas outside the focused campaign region for the period.
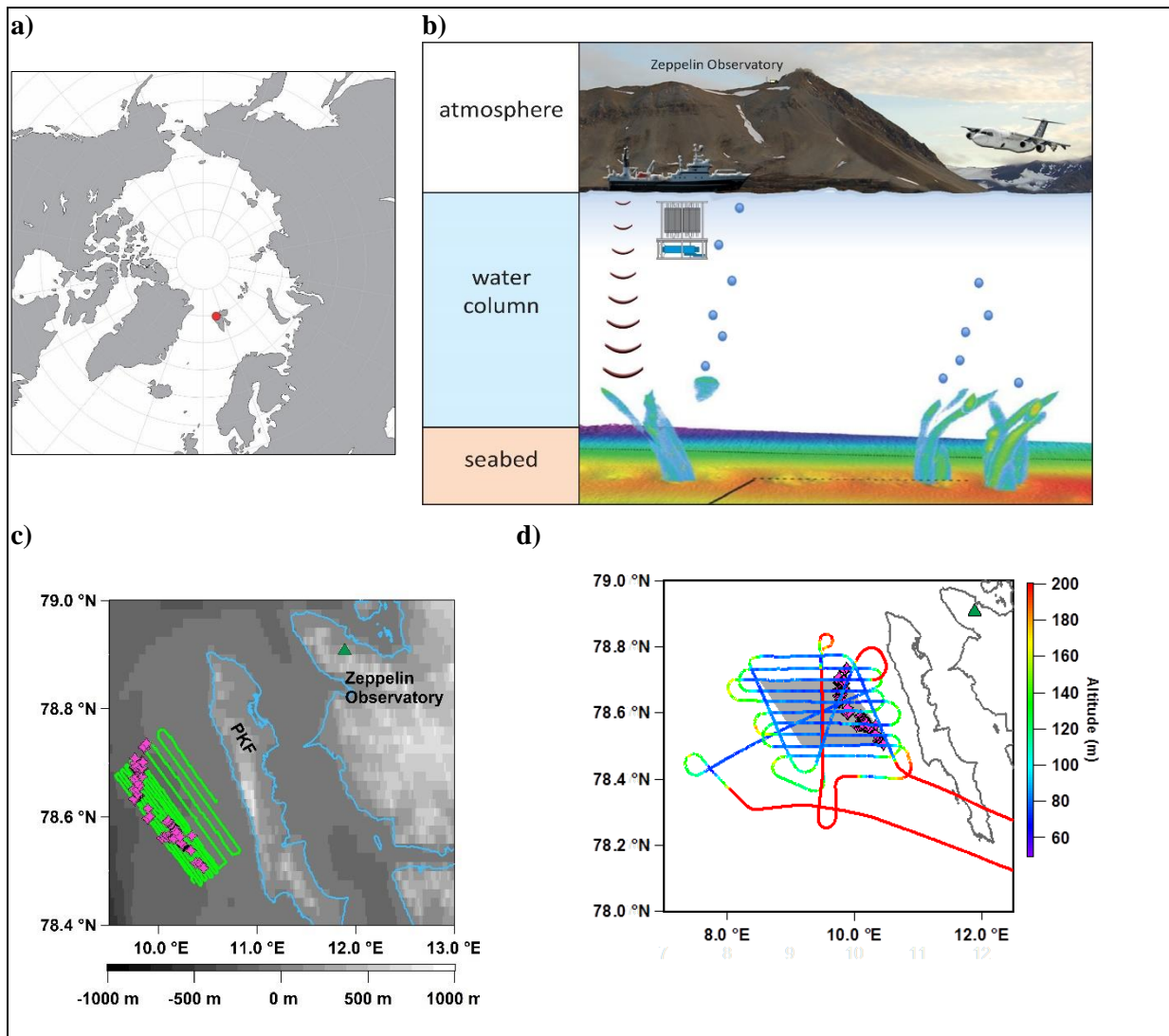
**Figure 1:** Field campaign and measurement platforms at the sea floor, in the water column, and in the atmosphere west of Svalbard in June-July 2014. a) The location of the measurement area marked in red west of Svalbard. b) Illustration of the field activity from 23 June to 2 July (not to scale) 2014. Seeps on the seafloor, represented here by swath bathymetry, release gas bubbles that rise through the water column. The Research Vessel Helmer Hanssen detected gas bubbles and collected water samples at various depths, and provided online atmospheric $CH_4$, CO and $CO_2$ mixing ratios and discrete sampling of complementary trace gases and isotopic ratios. The Facility of Airborne Atmospheric Measurements (FAAM) aircraft measured numerous gases in the atmosphere, and an extended measurement program was performed at the Zeppelin Observatory close to Ny-Ålesund. c) Detailed map of the area of intense ship-borne measurements. The ship track (green line) covers an Arctic shelf region, ~80-200 m depth, as indicated by bathymetric data west of Prins Karls Forland (PKF), an area with numerous observed flares [Westbrook et al, 2009; Sahling et al., 2014; and this work, shown as pink symbols]. The location of the Zeppelin observatory is shown (green triangle), ~50 km from PKF. d) Flight track over the same region on 2nd July; altitude is given by the colour scale, and the area used for the flux calculation based on flight data is shown in grey.

## 2   Data and Methodology

### 2.1   Field platforms, measurements and data

An overview of the area together with the complementary measurement platforms is presented in Figure 1. The Research Vessel (RV) Helmer Hanssen was equipped with instruments to analyse water samples from the sea surface down to the seabed and to monitor $CH_4$ atmospheric mixing ratios from 20 June an onwards. A single-beam echosounder constantly recorded flares in echograms; flares represent locations where bubbles are released from the seafloor which rise through the water column [Veloso et al., 2015], and where we expect high dissolved $CH_4$ concentrations. Figure 1c shows the ship's route during 24 -27  June 2014, together with identified gas flares. Aircraft measurements during the campaign were performed as low as ~15 m above the ocean, covering a larger area than the ship, for a short time (flights were around 4 h in duration).  Figure 1d shows the 'Facility of Airborne Atmospheric Measurements' (FAAM) aircraft path and height on 2 July 2014 in the area, and the location of the flares identified [see Pitt et al., 2016; O'Shea et al, 2013; Allen et al., 2011 for details of the aircraft and instrumentation]. Finally, measurements of the atmospheric composition at the nearby Zeppelin Observatory include continuous $CH_4$ measurement and daily sampling of $CH_4$ isotopic ratios, amongst others (see Table S1); Figure S1 shows the locations. A description of all instruments and methods employed is included in the supplementary information. Table S1 gives an overview of the instruments from all platforms involved.

### 2.2   Model tools for data analysis and top-down flux estimations

Potential $CH_4$ seep locations around Svalbard were determined by MH stability modelling. The MH stability model (CSMHYD program, Sloan and Koh, 2008) was used taking bottom water temperatures (World Ocean Database, 2013) and sediment thermal gradients (Global Heatflow Database) from around Svalbard as input parameters. Locations where the hydrate stability zone outcrops at the seabed, are considered to be potential $CH_4$ seep locations. These locations were supplemented with all known $CH_4$ seeps [this work, Sahling et al., 2014, Panieri et al, 2015]. The modelled potential methane seep locations and known methane seeps are illustrated in Figure 2 as light blue and red dots, respectively.
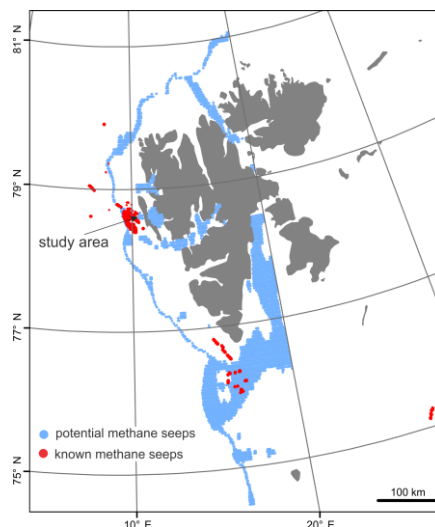
**Figure 2:** The identified (red) and potential (blue) seep locations around Svalbard as calculated by methane hydrate stability modelling.

138 In order to estimate $CH_4$ fluxes from the modelled seep area (blue in Figure 2) and identified
139 $CH_4$ seep areas (red in Figure 2), we used three different independent atmospheric models; [1] the
140 Lagrangian particle dispersion model FLEXPART [Stohl et al., 2005], [2] the global chemical
141 transport model Oslo CTM3 [ Søvde et al., 2012, Dalsøren et al., 2016], and [3] a Lagrangian mass
142 balance box model [Karion et al., 2013; O'Shea et al. 2014]. See section S3 for details about
143 models and simulations.
144

## 145  3   Results and Discussion

146 **3.1   Observations in the ocean and atmosphere**
147 We present the results following the methane migration path from the sea floor through the water
148 column into the lowermost atmosphere close to the sea surface (ship) and higher up using flight
149 data covering a larger area. Figure 3 illustrates the dissolved $CH_4$ concentrations sampled over
150 the investigated area. Elevated concentrations were found around the most extended cluster of
151 flares and the $CH_4$ distribution shows a rapid change at about ~50 m water depth, with the
152 highest dissolved $CH_4$ concentrations near the seafloor ~150 m depth. Little $CH_4$ is found above
153 the pycnocline (boundary where the density gradient is greatest, affected by temperature and
154 salinity), but sea surface $CH_4$ concentrations are still oversaturated with respect to atmospheric
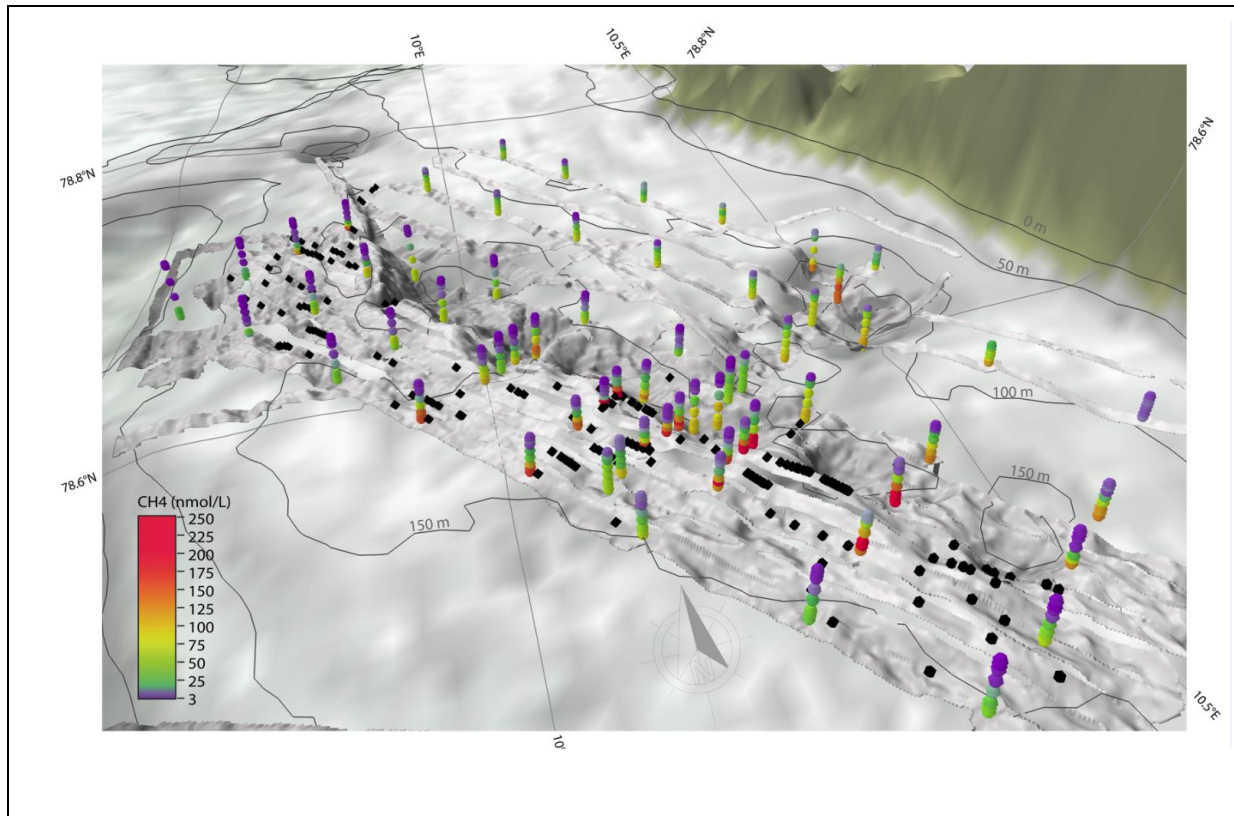155 concentrations in a few places eastward, close to the shore

**Figure 3:** $CH_4$ concentrations from a hydrocast survey offshore of Prins Karls Forland. The first three bottles were taken 5, 15 and 30 meters above the seafloor and the last three bottles were taken 10, 20 and 30 meters below the sea surface. The rest of the samples were spread equally in the water column depending on the bottom depth. $CH_4$ concentrations in the ocean are illustrated by coloured dots (scale on the bottom left in nmol $L^{-1}$). Black dots indicate the location of the gas flares. Isobaths are from IBCAO v.3 grid and the superimposed higher resolution bathymetry is from the multi-beam survey performed during the RV Helmer Hanssen cruise, data were recorded over the period 25 June – 1 July 2014.

156
157 The sea-surface $CH_4$ ocean concentrations (Figure 4a) and the atmospheric mixing ratio
158 measured by both the ship (Figure 4b) and the aircraft (Figure 4c) show very similar patterns. In
159 the surface water $CH_4$ was generally <8 nmol $L^{-1}$ (Figure 4a) with a median of 4.8 nmol $L^{-1}$. A
160 maximum of 26 nmol $L^{-1}$ was found near the shore, where no gas flares are found in the vicinity
161 (Figure 4 a/b). The elevated surface water $CH_4$ concentrations coincide with a small increase (<2
162 ppb) of atmospheric $CH_4$ mixing ratio detected by the ship. This slightly elevated $CH_4$ close to
163 the shore is probably not due to $CH_4$ released from the seafloor/seeps. Figure 3 and Figure 4
164 show that the bottom $CH_4$ concentrations are low in this coastal area. A simultaneous decrease in
165 salinity suggests the intrusion of methane-enriched fresher water [Damm et al., 2005] increasing
166 the dissolved sea surface-near $CH_4$ concentrations in this particular area.
167
168 A 6 km transect was sampled twice in one week by the *Helmer Hanssen* to monitor rapid
169 variations of oceanographic conditions and their effects on the dissolved $CH_4$ distribution. The
170 maximum bottom water $CH_4$ concentration doubled in one week from 200 to 400 nmol $L^{-1}$ (see

171    Figure 4d and S2) while bottom water temperatures remained relatively stable. At the same time,
172    the concentrations above the pycnocline and at sea surface remained relatively stable and low (4-
173    11 nmol L$^{-1}$ and ~10 nmol L$^{-1}$ in the surface water on 24$^{th}$ June and 1$^{st}$ July, respectively).
174
175    This is in agreement with changes reported by Steinle et al, [2015] for bottom and sea surface
176    water. This change in concentration can be explained either by slower advection during the later
177    observations, or that the water was previously CH$_4$ enriched by an emission burst from one or
178    several nearby seep sites. Gas bubble dissolution modelling from a previous study in the deeper
179    area to the west of our study area, estimated that 80% of the bubble released CH$_4$ is dissolved
180    below the summer pycnocline, and the remaining CH$_4$ is transported northwards where it is most
181    likely oxidised by methanotrophic bacteria [Gentz et al, 2014, Steinle et al. 2015]. A similar
182    conclusion came from a box modelling result of dissolved CH$_4$ indicating that ~60% of
183    CH$_4$released at the seafloor becomes already oxidized before it reaches the overlying surface
184    waters [ Graves et al., 2015]. Although our single beam echosounder studies show bubbles
185    reaching the sea surface, very little CH$_4$ remains in such bubbles by the time they reach the
186    surface [Greinert and McGinnies, 2009].
187
188    We compared data from the RV Helmer Hansen to those from the Zeppelin observatory for the
189    period from 20 June – 1 August. The CH$_4$ mixing ratio measured aboard the ship during the
190    measurements off PKF agrees well with those recorded by the Zeppelin Observatory, as does the
191    isotopic ratio (see Supplementary Figure S3). Our measurements above the flares were not
192    influenced by long range transport of methane-enhanced-air masses from lower latitudes, as this
193    would have produced noticeable transient enhancements in CH$_4$, as exemplified in Figure S3.
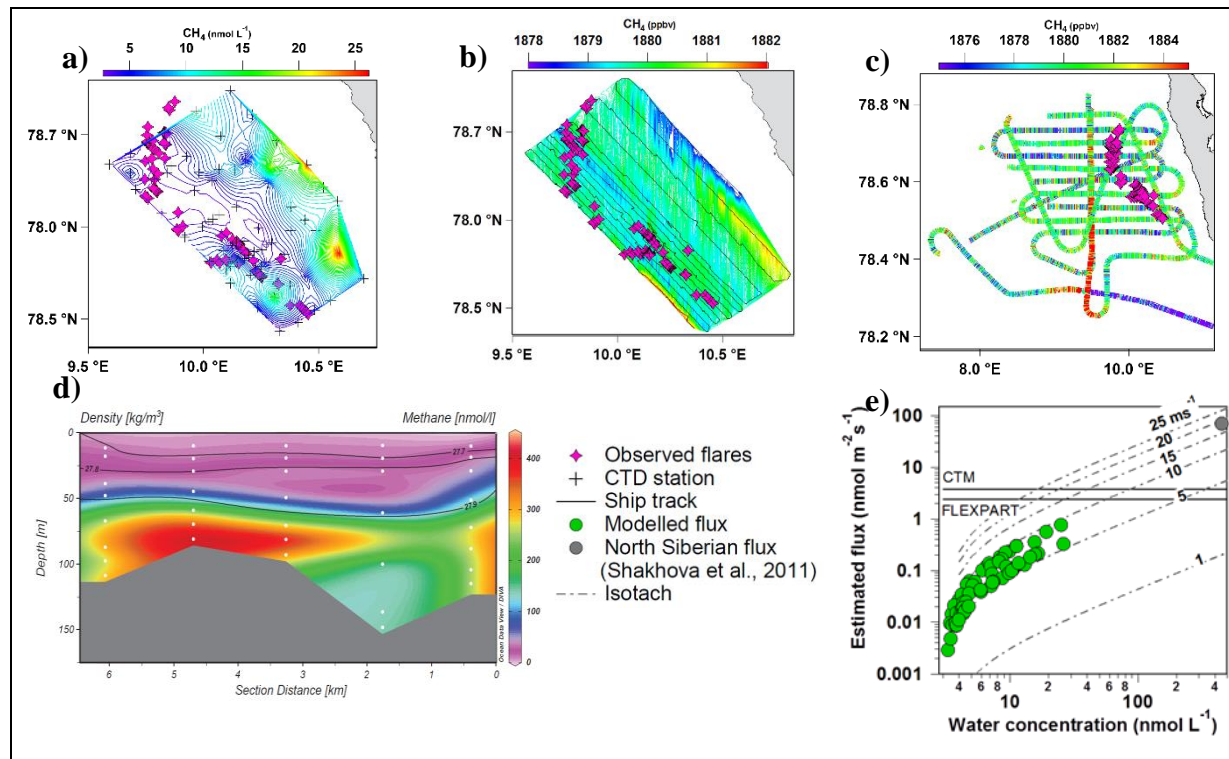
**Figure 4:** Comparison of CH4 variations in the ocean and atmosphere west of Svalbard, and corresponding CH4 flux to the atmosphere. a) Contour plot of near-surface CH4 concentration (colour scale) at ~10 m depth in the water column. *CH4* was measured by oceanographic conductivity/temperature/depth (CTD) stations (crosses) west of Prins Karls Forland (PKF). Observed flares are shown by pink markers. b) Contour plot of atmospheric CH4 mixing ratio in ppb measured aboard RV Helmer Hanssen (colour scale). Ship track shown by black line, flares are shown by pink markers. c) CH4 measured by the FAAM aircraft, flares are shown by pink markers. d) CH4 concentration in the water column along a transect of CTD stations taken on 1st July 2014 showing a clear stratification of water masses with the pycnocline near 50 m water depth. Density is own as black contours. (The transect location offshore of Prins Karls Forland is shown in Figure S2, b). Panel e) CH4 flux to the atmosphere at each CTD location as a function of ocean CH4 concentration according to a diffusive model (green points). Flux previously modelled off Northern Siberia during stormy weather [Shakhova et al., 2011] is given by the grey point. Dashed lines show the model flux at different isotachs (lines of constant wind speed), assuming constant salinity and temperature (averaged over the sampling period used). Horizontal lines show the maximum possible flux constrained by the atmospheric measurements from the ship, according to FLEXPART and OsloCTM3 models. FLEXPART and CTM constraints are for the atmospheric sampling period 20 June – 1 Aug and will vary with weather patterns.

194

**3.2    Flux estimates from ocean to atmosphere in the Svalbard region during summer**

We estimate the median ocean-atmosphere CH4 flux based on observations in the ocean, in addition to 3 top-down constrain of the flux employing 3 independent models and the atmospheric measurements.

199

200  We estimate a median ocean-atmosphere $CH_4$ flux of 0.04 nmol m$^{-2}$ s$^{-1}$ ($\sigma$ = 0.13) from data at
201  each *CTD* station using an ocean-atmosphere gas exchange function [Wanninkhof et al, 2009,
202  Figure 4e]. The maximum flux at the CTD stations is 0.8 nmol m$^{-2}$ s$^{-1}$ which occurred when both
203  dissolved $CH_4$ concentrations and wind speeds were high, 25 nmol L$^{-1}$ and 9 m s$^{-1}$ respectively.
204  This model only considers air-sea exchange via diffusion of dissolved $CH_4$ and not the
205  contribution of bubbles of gas reaching the surface. Figure 4e) shows the estimated flux at
206  different wind speeds, assuming constant salinity and temperature (average from the campaign).
207  Wind speed has a large effect: an increase from 5 to 10 ms$^{-1}$ increases the modelled flux by
208  almost an order of magnitude. The atmospheric $CH_4$ air mixing ratios aboard the RV Helmer
209  Hanssen and at Zeppelin before, during, and after the ship-based measurements off Prins Karls
210  Forland were very similar, with small variations (Figure 4e/b). Hence, the $CH_4$ air mixing ratios
211  above active seep areas were representative of wider regional atmospheric concentrations, with
212  no elevated levels or transient large increases.
213
214  To complement our observational based flux estimates of dissolved $CH_4$ we employed three
215  independent atmospheric models to provide top-down constraints of the ocean-atmosphere flux,
216  given the atmospheric concentrations sampled by the aircraft and the ship. This approach also
217  take potential $CH_4$ from bubbles into account. We only detected a weak increase of 2 ppb in the
218  atmospheric mixing ratio at the ship location close to bubbles, reflecting the potential
219  enhancement from both dissolved $CH_4$ and $CH_4$ from bubbles. We calculated, using a
220  Lagrangian transport model (FLEXPART), the $CH_4$ enhancements at the ship for all locations
221  that would result from a 1 nmol m$^{-2}$s$^{-1}$ flux from the area, encompassing the identified and the
222  potential $CH_4$ seep sites around Svalbard [Sahling et al., 2014, shown in Figure 2]. Running
223  FLEXPART backwards in time for all ship positions over the period 20 June to 1 August, the
224  modelled $CH_4$ enhancement is shown as the yellow line in the supplementary section, Figure S4;
225  compared to the observations, no correlation (r$^2$=0.003) is evident. The most sensitive days are
226  the highest 20% modelled peaks, (bold yellow line). Using the most sensitive days from this
227  period we estimate a top down constraint on the flux from the seep areas of <2.4±1.3 nmol m$^{-2}$ s$^{-1}$
228  . This estimation assumes that all of the measured 2 ppb variation in the atmosphere is solely
229  due to a flux from the modelled seep areas around Svalbard (Figure 2). Similarly, using a
230  forward chemistry transport model (OsloCTM3, Søvde et al., 2012) a flux of 3.8 ±0.7 nmol m$^{-2}$
231  s$^{-1}$ was necessary to reproduce the 2 ppb increase in $CH_4$ at the ship, assuming the same emission
232  region shown in Figure 2. This is equivalent to an annual emission of only 0.06 Tg for a constant
233  flux throughout the year, very small compared to the total global annual emission of ca 600 Tg of
234  $CH_4$, [Kirschke et al. 2013]. In addition, we used the aircraft measurements to provide another
235  independent constrain on the maximum possible $CH_4$ flux in the region. The aircraft flew
236  transects below 100 m altitude upwind and downwind of the potential seep sites, but observed no
237  statistically significant change in $CH_4$ during these low level flights, see Figure 1d for altitudes.
238  A Lagrangian mass balance calculation (similar to that employed by O'Shea et al., 2014) leads to
239  an estimated flux of 3.0 ± 17.1 nmol m$^{-2}$ s$^{-1}$. An estimated upper limit on the ocean-to-
240  atmosphere $CH_4$ flux averaged over the grey shaded area shown in Figure 1d can then be
241  quantified by the mean + 1$\sigma$ value of 14.1 nmol m$^{-2}$ s$^{-1}$. This represents the maximum possible
242  flux for this area consistent with the aircraft $CH_4$ measurements and associated uncertainties.
243
244  FAAM aircraft measurements were also made in the same location off PKF in a previous
245  MAMM campaign in summer 2012 as part of the UK Methane in the Arctic Measurement and
246  Modelling project (MAMM – see Allen et al., 2014 for details). Similarly, any emission from the

247  seep areas was not detectable among the other signals in the aircraft data. Forward calculations,
248  with a different dispersion model, led to very similar conclusions to those of 2014: that an
249  emission flux of a few tens of nmol m$^{-2}$ s$^{-1}$ would have been required to detect the emission in
250  the aircraft data [M. Cain, personal communication, 2016].
251
252  In sharp contrast to the flux calculations from the measurement-led approaches discussed here
253  (Table 1), the flux reported by Shakhova et al. [2014] from the East Siberian Arctic Shelf is more
254  than two orders of magnitude larger, 70-450 nmol m$^{-2}$ s$^{-1}$ under windy conditions, than our
255  measurement-derived maximum for the period. Figure 4, panel e includes a comparison. Part of
256  this large difference can be explained by both higher dissolved CH$_4$ concentrations in surface
257  waters reported in the Siberian area (up to ~400 nmol L$^{-1}$) and the higher wind speeds reported
258  by Shakhova et al. [2014]. Table 1 compiles our estimates of the spatially-averaged maximal flux
259  in the region, as constrained by the atmospheric observations.
260
261

**Table 1:** Ocean to atmosphere CH$_4$ flux constraints offshore Prins Karls Forland from different independent methodologies. The potential flux region is shown in Figure 2, and employing atmospheric observation from Zeppelin and Helmer Hanssen over the period 20 June – 1 August 2014

| *Methodology* | *Maximum flux possible constrained by the atmospheric observations* |
|---|---|
| | **(nmol m$^{-2}$ s$^{-1}$)** |
| *FLEXPART[a] top-down, backward modelling* | *2.4 ± 1.4* |
| *OsloCTM3[b] top-down forward modelling* | *3.8 ± 1.4* |
| *Lagrangian mass balancing - FAAM)[c], top-down, exploring up-wind/down-wind variations* | *14.1* |

262  [a] *Lagrangian Particle Dispersion model [Stohl et al., 2005]* [b] *Chemical transport model [Søvde et al. 2012, Dalsøren et al 2016]* [c]
263  *Lagrangian mass balance approach [Karion et al., 2013; O'Shea et al. 2014]. Note that the flux constrain based on the flight data*
264  *is weaker; there was no statistically significant change in downwind CH$_4$ mixing ratio relative to the measured upwind*
265  *background, and this is the maximum possible flux that is consistent with the atmospheric flight measurements and associated*
266  *uncertainties.*
267

## 4 Conclusion

269  Despite the obvious influence of seeps on dissolved CH$_4$ concentrations in the ocean west of
270  Svalbard in June - July summer 2014, very little CH$_4$ reaches the atmosphere, neither as bubbles
271  transported nor dissolved gas. The median wind speed was 6.6 m s$^{-1}$ during our campaign, and
272  the pycnocline remained stable. We suggest that dissolved methane captured below the
273  pycnocline may only be released to the atmosphere when physical processes remove this
274  dynamic barrier. In such a situation, dissolved CH$_4$ concentrations would rapidly decrease and
275  any large flux would most likely be transient. Consequently, we conclude that large CH$_4$ releases
276  to the atmosphere with strong impact on the atmospheric levels from sub-sea sources, including
277  hydrates, do not occur to the west of Svalbard, presently. Shorter periods with large fluxes,
278  particular during other times of the year such as during ice break-up or storm events, might

279  occur. The role of the pycnocline in this context will be investigated in more detail during long-
280  term ocean observatory recordings in the future.
281
282

291
292
293

## Supporting Information
294
295
296

## References
298  Allen, G., Coe, H., Clarke, A., Bretherton, C., Wood, R., Abel, S. J., Barrett, P., Brown, P.,
299      George, R., Freitag, S., McNaughton, C., Howell, S., Shank, L., Kapustin, V., Brekhovskikh,
300      V., Kleinman, L., Lee, Y.-N., Springston, S., Toniazzo, T., Krejci, R., Fochesatto,J., Shaw,
301      G., Krecl,P., Brooks, B., McMeeking, G., Bower, K. N., Williams, P. I., Crosier, J., Crawford
302      I., Connolly, P., Allan, J. D., Covert, D., Bandy, A. R., Russell, L. M., Trembath, J., Bart, M.,
303      McQuaid, J. B., Wang, J., and Chand, D.: South East Pacific atmospheric composition and
304      variability sampled along 20° S during VOCALS-REx, *Atmos. Chem. Phys*., 11, 5237-5262,
305      doi:10.5194/acp-11-5237-2011, 2011.
306  Allen, G., Illingworth, S. M., O'Shea, S. J., Newman, S., Vance, A., Bauguitte, S. J.-B.,
307      Marenco, F., Kent, J., Bower, K., Gallagher, M. W., Muller, J., Percival, C. J., Harlow, C.,
308      Lee, J., and Taylor, J. P.: Atmospheric composition and thermodynamic retrievals from the
309      ARIES airborne TIR-FTS system – Part 2: Validation and results from aircraft campaigns,
310      Atmos. Meas. Tech., 7, 4401-4416, doi:10.5194/amt-7-4401-2014, 2014.
311  Archer, D. Methane hydrate stability and anthropogenic climate change. *Biogeosciences* **4,** 521–
312      544 (2007).
313  Berchet, A., Bousquet, P., Pison, I., Locatelli, R., Chevallier, F., Paris, J.-D., Dlugokencky, E. J.,
314      Laurila, T., Hatakka, J., Viisanen, Y., Worthy, D. E. J., Nisbet, E., Fisher, R., France, J.,
315      Lowry, D., Ivakhov, V., and Hermansen, O.: Atmospheric constraints on the methane
316      emissions from the East Siberian Shelf, Atmos. Chem. Phys., 16, 4147-4157,
317      doi:10.5194/acp-16-4147-2016, (2016) 2016.
318  Biastoch, A. *et al.* Rising Arctic Ocean temperatures cause gas hydrate destabilization and ocean
319      acidification. *Geophys. Res. Lett.* **38**, L08602, doi:10.1029/2011gl047222 (2011).
320  Bugna, G.C., J.P. Chanton, J.E. Young, W.C. Burnett and P.H. Cable. The importance of
321      groundwater discharge to the methane budget of nearshore and continental shelf waters of the
322      NE Gulf of Mexico Geochimica et Cosmochimica Acta, 60, 4735-4746 (1996).
323  Ciais, P. *et al.* Carbon and other biogeochemical cycles. In: *Climate Change 2013 – The Physical*
324      *Science Basis*. pp. 465-570. Cambridge: Cambridge University Press (2014).

325 Collins, M. *et al.* Long-term climate change: projections, commitments and irreversibility. In:
326     *Climate Change 2013 – The Physical Science Basis*. pp. 1029-1136. Cambridge: Cambridge
327     University Press (2014).
328 Dalsøren, S. B., Myhre, C. L., Myhre, G., Gomez-Pelaez, A. J., Søvde, O. A., Isaksen, I. S. A.,
329     Weiss, R. F., and Harth, C. M.: Atmospheric methane evolution the last 40 years, *Atmos.*
330     *Chem. Phys.*, 16, 3099-3126, doi:10.5194/acp-16-3099-2016 (2016)
331 Damm, E., Mackensen, A., Budeus, G., Faber, E. & Hanfland, C. Pathways of methane in
332     seawater: Plume spreading in an Arctic shelf environment (SW-Spitsbergen). *Continent. Shelf*
333     *Res*. **25**, 1433–1452 (2005).
334 Ferré, B., Mienert, J. & Feseker, T. Ocean temperature variability for the past 60 years on the
335     Norwegian-Svalbard margin influences gas hydrate stability on human time scales. *J.*
336     *Geophys. Res.: Oceans* **117**, C10017, doi:10.1029/2012jc008300 (2012).
337 Fisher, R. E. *et al.* Arctic methane sources: Isotopic evidence for atmospheric inputs. *Geophys.*
338     *Res. Lett.* 38**,** L21803, doi:10.1029/2011GL049319 (2011).
339 Gentz, T. *et al.* A water column study of methane around gas flares located at the West
340     Spitsbergen continental margin, *Continent. Shelf Res.* **72,** 107–118 (2014).
341 Graves, C. A. et al. Fluxes and fate of dissolved methane released at the seafloor at the landward
342     limit of the gas hydrate stability zone offshore western Svalbard. . *J. Geophys. Res.* Oceans
343     **120,** doi:10.1002/2015JC011084 (2015).
344 Greinert, J. & McGinnis, D.F. Single bubble dissolution model - the graphical user interface
345     SiBu-GUI. *Environ. Model. Software* **24**, 1012-1013 (2009).
346 Isaksen, I.S.A, Gauss, M., Myhre, G., Walter Anthony, K. M. & Ruppel, C. Strong atmospheric
347     chemistry feedback to climate warming from Arctic methane emission. *Global Biogeochem.*
348     *Cy.*, **25**, GB2002, doi:10.1029/2010GB003845 (2011).
349 Karion, A., *et al.* Methane emissions estimate from airborne measurements over a western
350     United States natural gas field. *Geophys. Res. Lett.* **40**, 4393-4397 (2013).
351 Kirschke, S. *et al.* Three decades of global methane sources and sinks. *Nature Geosci.* **6**, 813-
352     823 (2013).
353 Knies, J., Damm, E., Gutt, J., Mann, U. & Pinturier, L. Near-surface hydrocarbon anomalies in
354     shelf sediments off Spitsbergen: Evidences for past seepages. *Geochem. Geophys. Geosyst.* **5,**
355     Q06003, doi:10.1029/2003GC000687 (2004).
370 McGinnis, D. F., J. Greinert, Y. Artemov, S. E. Beaubien, and A. Wüest, Fate of rising methane
371     bubbles in stratifiedwaters: How much methane reaches the atmosphere?, *J. Geophys. Res.,*
372     **111**, C09007, doi:10.1029/2005JC003183 (2006).
373 Myhre, G. *et al.* Anthropogenic and natural radiative forcing. In: *Climate Change 2013 – The*
374     *Physical Science Basis*. pp. 659-740. Cambridge: Cambridge University Press (2013).
375 Nisbet, E. G., Dlugokencky, E. J. & Bousquet, P. Methane on the rise — again. *Science* **343**,
376     493-495 (2014).
377 Nordlie, Ø, Przybylak, R., Ogilvie, A. E. J. & Isaksen, K. Long-term temperature trends and
378     variability on Svalbard: the extended Svalbard Airport temperature series, 1898-2012. *Polar*
379     *Res.* **33**, 21349, doi:10.3402/polar.v33.21349, 2014.
380 O'Shea, S. J., Bauguitte, S. J.-B., Gallagher, M. W., Lowry, D. & Percival, C. J. Development of
381     a cavity-enhanced absorption spectrometer for airborne measurements of $CH_4$ and $CO_2$.
382     *Atmos. Meas. Tech.* **6**, 1095-1109 (2013).
383 O'Shea, S. J. *et al.* Area fluxes of carbon dioxide, methane, and carbon monoxide derived from
384     airborne measurements around Greater London: A case study during summer 2012. *J.*
385     *Geophys. Res.: Atmos.* **119**, 4940-4952 (2014).

386 Panieri et al., Gas hydrate deposits and methane seepages offshore western Svalbard and
387     Storfjordrenna: Biogeochemical and biological investigations, CAGE15-2 cruise report
388     (2015).
389 Panieri, G., Graves, C.A., James, R.H., Paleo-methane emissions recorded in foraminifera near
390     the landward limit of the gas hydrate stability zone offshore western Svalbard. G3,
391     Geochemistry, Geophysics, Geosystems, DOI: 10.1002/2015GC006153 (2016).
392 Pitt, J. R. *et al*. The development and evaluation of airborne in situ $N_2O$ and $CH_4$ sampling using
393     a quantum cascade laser absorption spectrometer (QCLAS). *Atmos. Meas. Tech.* **9,** 63-77
394     (2016).
395 Portnov, A., Vadakkepuliyambatta, S., Mienert, J., Hubbard, A., Ice-sheet driven methane
396     storage and release in the Arctic. Nature Communication; 7:10314, DOI:
397     10.1038/ncomms10314 (2016).
398 Portnov, A. *et al.* Offshore permafrost decay and massive seabed methane escape in water depths
399     >20 m at the South Kara Sea shelf. *Geophys. Res. Lett.* **40,** 3962–3967 (2013).
400 Rajan, A., Mienert, J. & Bünz, S. Acoustic evidence for a gas migration and release system in
401     Arctic glaciated continental margins offshore NW-Svalbard. *Mar. Petrol. Geol.* **32,** 36–49
402     (2012).
403 Ruppel, C. D. Methane hydrates and contemporary climate change. *Nature Education*
404     *Knowledge* **3**,10, 29, http://www.nature.com/scitable/knowledge/library/methane-hydrates-
405     and-contemporary-climate-change-24314790 (2011).
406 Sahling, H. *et al.* Gas emissions at the continental margin west of Svalbard: mapping, sampling,
407     and quantification. *Biogeosciences* **11**, 6029-6046 (2014).
416 Shakhova, N. *et al.* Geochemical and geophysical evidence of methane release over the East
417     Siberian Arctic Shelf. *J. Geophys. Res.* **115,** C08007, doi:10.1029/2009JC005602 (2010).
418 Shakhova, N. *et al.* Ebullition and storm-induced methane release from the East Siberian Arctic
419     Shelf. *Nature Geosci.* **7,** 64–70 (2014).
420 Sloan, E. D. & Koh, C. A. Clathrate Hydrates of Natural Gases, Third Edition. Boca Raton, FL.:
421     CRC Press (2008).
422 Smith, A.J., Mienert, J., Bünz, S. & Greinert, J. Thermogenic methane injection via bubble
423     transport into the upper Arctic Ocean from the hydrate-charged Vestnesa Ridge, Svalbard.
424     *Geochem. Geophys. Geosyst.* **15,** 1945-1959 (2014).
425 Steinle, L. *et al.* Water column methanotrophy controlled by a rapid oceanographic switch.
426     *Nature Geosci.* **8**, 378-382 (2015).
427 Stohl, A., Forster, C., Frank, A., Seibert, P., & Wotawa, G. Technical note : The Lagrangian
428     particle dispersion model FLEXPART version 6.2. *Atmos. Chem. Phys.* **5,** 2461-2474 (2005).
429 Søvde, O. A. *et al.* The chemical transport model Oslo CTM3. *Geosci. Model Dev.* **5,** 1441-1469
430     (2012).
431 Thompson, R. L., & Stohl, A. FLEXINVERT: an atmospheric Bayesian inversion framework for
432     determining surface fluxes of trace species using an optimized grid. *Geophys. Mod. Dev.* **7,**
433     2223-2242 (2014).
434 Veloso, M., Greinert, J., Mienert, J. & De Batist, M. A new methodology for quantifying bubble
435     flow rates in deep water using split beam echosounder: examples form the Arctic offshore
436     NW Svalbard. *Limnol. Oceanogr. Meth.*, doi:10.1002/lom3.10024 (2015).
437 Westbrook, G. K. *et al.* Escape of methane gas from the seabed along the West Svalbard
438     continental margin. *Geophys. Res. Lett.* **36**, L15608, doi:10.1029/2009gl039191 (2009).
439 Wanninkhof, R. *et al.* Advances in quantifying air-sea gas exchange and environmental forcing.
440     *Annu. Rev. Marine. Sci.* **1,** 213-244 (2009).

441    Whitemann, G., Hope, C., & Wadhams, P. Climate science: Vast costs of Arctic change. *Nature*
442        **499**, 401–403 (2013).
443    Wiesenburg, D. A. & Guinasso, N. L. Jr. Equilibrium solubilities of methane, carbon monoxide,
444        and hydrogen in water and sea water. *J. Chem. Eng. Data* **24**, 356-360 (1979.)